
Machine Learning Interatomic Potentials: Advancing Open-Source Software for Efficient and Scalable Molecular Simulation

Christoph Brunken Titouan Cormier Lucien Walewski Marco Carobene
Yessine Khanfir Zachary Weller-Davies Miguel Bragança Armand Picard
Adrien Pichard Leon Wehrhan Heloise Chomet Eszter Varga-Umbrich
Marie Bluntzer Massimo Bortone Valentin Heyraud Silvia Acosta-Gutiérrez
Jules Tilly Olivier Peltre

InstaDeep

1 Triton Square, London, NW1 3BF, United Kingdom
{c.brunken,j.tilly,o.peltre}@instadeep.com

Abstract

Machine learning interatomic potentials (MLIPs) enable atomistic simulations with near *ab initio* accuracy at significantly reduced computational cost, but their broader adoption is often limited by fragmented tooling, limited scalability, and inflexible software design. We present *mlip v2*, a new generation of the *mlip* library that advances efficient and scalable molecular simulation through a unified and extensible framework. The new release features a targeted API redesign with improved modularity and control, enabling flexible customization of training, data processing, and simulation workflows. It further integrates a new high-performance backend for equivariant operations, *e3j*, significantly accelerating model inference and simulations. In addition, the framework introduces a range of entirely new capabilities, including the eSEN architecture with a Mixture-of-Experts formulation for scalable training on large and diverse datasets, improved handling of electrostatics through more physically grounded charge modeling and long-range interaction treatment, and advanced simulation features such as NPT ensembles and nudged elastic band methods. Together, these extensions significantly broaden the scope of MLIP applications, enabling efficient modeling of complex, reactive, and out-of-equilibrium systems, and bridging the gap between ML research and practical molecular simulation applications. The library is available on GitHub and on PyPI under the Apache license 2.0.

1 Introduction

Machine learning interatomic potentials (MLIPs) have emerged as a powerful approach for atomistic simulation, enabling near *ab initio* accuracy at significantly reduced computational cost. By learning effective energy and force representations from quantum mechanical data, e.g., density functional theory (DFT), MLIPs provide a practical alternative to traditional force fields while remaining orders of magnitude faster than electronic structure methods. However, the adoption and development of MLIPs in practice are often hindered by the lack of unified, high-quality software infrastructure that supports (i) efficient simulation, (ii) ease of use for applications, and (iii) rapid methodological innovation.

To address this gap, the *mlip* library [1] was introduced in May 2025, a unified framework for training and deploying MLIP models, e.g., in molecular dynamics (MD) simulations. The library is entirely based on JAX, benefiting from just-in-time XLA (Accelerated Linear Algebra) compilation, and the efficient integration with the JAX-MD simulation backend [2] allowing for state-of-the-art molecular dynamics (MD) simulation speeds. The *mlip* library has since seen broad adoption, with thousands of downloads and usage in a growing number of downstream research projects (for example, see Ref. [3–5]). This first version of the library demonstrated the feasibility of a unified software stack that connects model training, inference, and molecular simulation in an efficient and easy-to-adopt framework to enable rapid prototyping and testing of novel ideas in the field of MLIPs. Moreover, it supports data-parallel training (even on a multi-host setup) on GPUs and TPUs, as well as batched inference, batched MD simulations, and batched energy minimizations. The library was also integrated into MLIPAudit, a JAX-compatible benchmarking toolset for MLIPs [6].

While version 1 (v1) provides a strong foundation for MLIP development, it was designed as a first-generation system, and naturally left room for further expansion. In this work, we present *mlip* v2, a new generation of the *mlip* library that addresses limitations through a targeted redesign, while preserving familiar interfaces and usage patterns. The redesigned architecture improves composability and control across end-to-end MLIP pipelines, including data processing, training, and molecular simulation. It also integrates *e3j*, a fully open-source high-performance backend for equivariant operations, with dedicated CUDA and Pallas kernels enabling significantly faster inference and MD simulations on both GPUs and TPUs (due for full release in June 2026).

Beyond performance and usability improvements, *mlip* v2 significantly expands the scope of supported methodologies and scientific applications:

1. **Model architectures:** In addition to the models already included in v1, we integrate the eSEN [7–9] architecture with an optional Mixture-of-Experts formulation, enabling scalable training on large and diverse datasets while preserving efficient inference. Most methods, embeddings, activations and layers are now interchangeable between model architectures, maximizing modularity for novel method development.
2. **Scientific capabilities:** The framework further extends its capabilities with support for advanced simulation and training paradigms, including NPT ensemble simulations (isothermal-isobaric), Hessian-label model training, and nudged elastic band (NEB) methods for transition state search.
3. **Charge predictions and electrostatics:** All models now support atomic partial charge prediction, and the treatment of electrostatics is significantly improved through explicit charge conditioning and long-range interaction modeling, enabling more physically faithful representations of charged systems.
4. **Fine-tuning:** Finally, multi-head fine-tuning is generalized across architectures, improving flexibility and consistency when adapting pretrained models to downstream tasks.

Overall, *mlip* v2 substantially expands the capabilities and performance of the *mlip* framework while introducing a more modular and flexible architecture for future research and development. The API has been redesigned to improve composability and extensibility while preserving a familiar interface for core workflows and minimizing breaking changes. To support adoption, we also provide

a comprehensive migration guide from v1. Together, these improvements establish *mlip* v2 as a scalable and adaptable foundation for ML-based molecular simulation.

2 Background and related work

MLIPs have rapidly placed themselves among the most promising AI based avenues for enhancing molecular discovery, spanning across materials discovery, bio-molecular sciences, and chemical engineering. In this library, we have so far focused on families of models based on Graph Neural Networks (GNNs) that preserve physical symmetries – at the very least invariance to rotation and translations in energy predictions, but oftentimes also equivariance of spatial output and latent information throughout the network. While equivariance usually comes at a computational cost, it has also been shown to improve data efficiency and stability in simulations [10, 11].

A first example of symmetry-preserving methods includes distance-based or invariant GNNs. These methods rely on interatomic distances to learn rotationally invariant energy predictions (e.g., SchNet [12–14], AIMNet2 [15], Crystal Graph Convolutional Neural Network [16]). To achieve equivariance, one needs to preserve geometric information throughout the network, for instance, by equivariantly updating edge features between each message passing layers [17] or guaranteeing inter-layer equivariance through computation of angular features (e.g., DimeNet [18, 19], GemNet [20, 21], ViSNet [22, 23]). This can also be achieved through general steerable 3D convolutions, generally built on the formalism of Clebsch-Gordan tensor products [24–26] to achieve arbitrary orders of representation of geometric features (e.g., NequIP [10], the Tensor Field Network [27], MACE [28–32]). Some approaches have also proposed a modified version of the tensor product to achieve higher computational efficiency, such as projections to a 2D domain for faster convolutions, such as eSEN [7–9, 33], or by rewriting the tensor product as integrals of the feature vectors’ corresponding signal on a sphere [34–36]. Finally, multiple transformer based methods have also been developed to strictly preserve equivariance (see, e.g., Ref. [37–40]), or to learn it based on data augmentation or targeted loss constraints (see, e.g., Ref. [41, 42]).

3 Library overview and updates

3.1 Design philosophy

In its first version, the *mlip* library was designed as an end-to-end toolbox for MLIP models, covering the full workflow from data processing and model development to training and deployment in inference tasks such as MD simulations. The design was guided by three core principles. First, **ease of use** was prioritized to lower the barrier to entry for application-focused non-expert users, e.g., by providing sensible default configurations and extensive tutorials. Second, **extensibility** was enabled through a modular architecture that decouples the core building blocks of an end-to-end MLIP pipeline, connected via minimal, clearly defined interfaces. Third, **inference efficiency** was treated as a key priority, as we identified it as an essential factor for pushing MLIP models towards relevant industrial applications, in particular, in computational biology. This is realized through the tight integration of our JAX-based models with the JAX-MD simulation backend, along with native support for batched simulations, energy minimization, and inference workloads.

With continued development and broader usage of the library, we identified several opportunities to further improve the original design, particularly with respect to extensibility. While the modular structure of *mlip* v1 enabled a range of customization options, certain components, such as model call signatures, proved less flexible than desired for emerging advanced use cases and the new features introduced in this work. Similarly, the data processing pipeline was primarily optimized for standard training workflows, and extending it to more complex scenarios such as inference-specific preprocessing, multi-dataset training, or multi-head fine-tuning required additional effort. In addition, many model implementations were initially adapted from existing open-source projects, which allowed for rapid development but did not fully exploit the potential for reusable building blocks and a consistent architectural pattern. These observations motivated a set of targeted API

and implementation refactors in *mlip* v2, aimed at improving flexibility and making the library a more powerful and convenient toolbox for both applied users and researchers developing new or customized MLIP models.

On the performance side, our focus on inference efficiency led to the identification of new requirements, in particular the need for a custom low-level backend to further optimize execution times. This motivated the development and integration of *e3j* into the library.

At the same time, we place a strong emphasis on maintaining a stable and familiar user experience. Despite internal changes, the overall structure and feel of the API remain largely consistent, with only minimal adjustments for existing users. In this sense, v2 is designed to make the library more powerful and flexible for advanced users, while preserving the simplicity and usability that applied researchers rely on, and also delivering tangible benefits for them in the form of significant speed improvements and additional features.

3.2 Usage and migration

mlip v2 has been released as version 0.2.0 of the library on GitHub¹ and PyPI² in May 2026, and can be installed easily via `pip`.

A detailed overview of API and code updates can be found either in our extensive migration guide that is part of our code documentation³ or in Appendix A. As mentioned above, for most applied research workflows, migration from v1 to v2 will require minimal effort.

A central component of the redesigned v2 code base is the introduction of a unified `Graph` class, which replaces the previously used `jraph.GraphsTuple` objects. This change removes the dependency on *jraph* [43], a project archived in May 2025, and provides a more maintainable and future-proof foundation. Beyond this, the `Graph` class offers a more expressive and well-documented representation of graph data, with built-in methods for common operations such as computing edge vectors from stored positions and connectivity. In v2, it serves as the core data structure throughout the library, consistently representing model inputs, outputs, and even optionally intermediate latent features. This unified representation allows us to standardize all major model components around a `Graph → Graph` interface, leading to cleaner composition of model blocks and greater flexibility in designing and reusing architectures. Finally, its object-oriented design makes it straightforward for advanced users to extend via inheritance (e.g., to add new input or output features), while updated data processing pipelines follow similar patterns, allowing customization with minimal code duplication.

Building on these changes, all core model implementations in v2 were refactored with this unified design in mind, adopting consistent interfaces and reusable building blocks. In addition, we integrated the *e3j* library to accelerate MACE and NequIP models (see section 4). For backwards compatibility, the original v1 model implementations are still available within a dedicated module. However, they are now exposed through the updated and slightly extended v2 `ForceField` interface, ensuring that models trained with the previous codebase remain usable. We note that this support is intended as a transitional solution, and plan to phase out the legacy implementations in future releases as part of ongoing efforts to simplify and modernize the code base.

4 Accelerating equivariant operations with *e3j*

In order to optimize runtime on a large span of hardware, the library supports the open-source *e3j* backend. The backend includes dedicated kernels for equivariant operations in both Pallas and CUDA for efficient implementation of MLIP models across both TPUs and GPUs.

This is particularly relevant for MACE and NequIP, which both rely on the Clebsch-Gordan Tensor Product for their internal operations, which usually constitute a significant computational bottleneck.

¹<https://github.com/instadeepai/mlip>

²<https://pypi.org/project/mlip>

³<https://instadeepai.github.io/mlip>

We include with the library examples of training MACE and NequIP with the *e3j* backend. These achieve consistent performance boost over the previous version of the library (up to 3x). See Figure 1 for an end-to-end runtime benchmark. It is worth noting that the version of *e3j* deployed in the *mlip* library is still work in progress. Further work is ongoing to improve fusion of the message passing kernel which should bring additional speed-ups an ability to scale model deployment to larger systems.

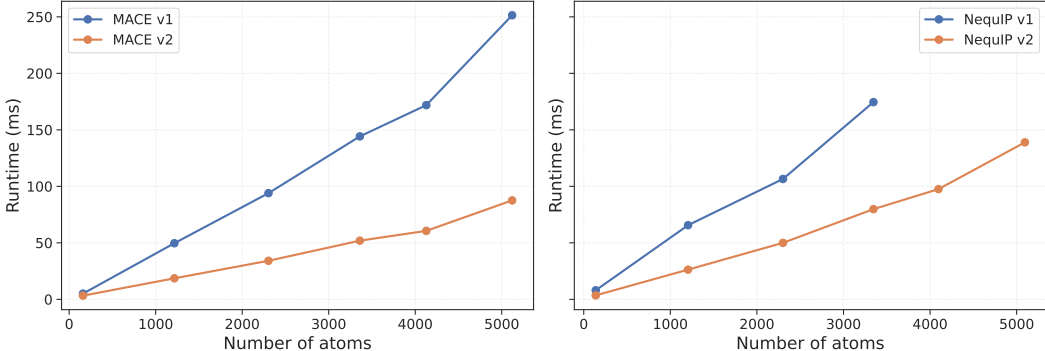


Figure 1: Results of end-to-end runtime benchmarks on MACE and NequIP, comparing the *mlip* v1 and *mlip* v2 versions, showcasing clear speed-ups across the board for both models. For this visualization, we show the Pallas implementation for MACE and the CUDA one for NequIP, as these represent the fastest options at the time of this writing. Further speed-up and scale should be expected following the full release of the *e3j* library.

5 Extended Scientific Capabilities

5.1 Treatment of electrostatics and long-range interactions

We introduce new electrostatics capabilities in *mlip* v2, aimed at improving the modeling of physically relevant interactions. In particular, the library now supports enhanced treatment of long-range electrostatic effects as well as global charge conditioning, enabling more accurate and flexible simulations of charged systems. In the following, we describe these two components in more detail.

Different approaches to modeling long-range interactions in MLIPs have been proposed in the literature [32, 44–46], where models typically rely on self-predicted atomic partial charges to compute the Coulomb electrostatic contribution E_{LR} to the total energy. Atomic partial charges are obtained via supervised learning, where reference charges (derived from a chosen electronic structure method) are used as targets in the loss function. To ensure physical consistency, the predicted partial charges q_i are constrained such that their sum matches the total system charge Q_{tot} , thereby guaranteeing charge conservation,

$$\tilde{q}_i = q_i - \frac{1}{N_S} \left(\sum_{j \in S} q_j - Q_{tot} \right) . \quad (1)$$

Here, \tilde{q}_i denotes the corrected partial charge of atom i , q_i the raw predicted charge, S the set of atoms in the system, and N_S its cardinality. *mlip* v2 currently implements a modified Coulomb interaction term E_{LR} to account for long-range electrostatic interactions, following the formulation introduced in PhysNet [44],

$$E_{LR} = \sum_{i,j \in S} k_e \frac{\tilde{q}_i \tilde{q}_j}{\chi(r_{ij})} , \quad (2)$$

Here, $k_e = \frac{1}{4\pi\epsilon_0}$ is Coulomb’s constant, with ϵ_0 denoting the vacuum permittivity, and r_{ij} the distance between atoms i and j . To avoid divergences of the Coulomb interaction at short interatomic distances, a modified distance function $\chi(r_{ij})$ is used. This surrogate distance matches the true distance r_{ij} beyond a soft-core radius r_0 , while smoothly regularizing the interaction at shorter distances, as proposed in PhysNet [44].

We emphasize that the new modular API design also makes it straightforward to add custom energy heads, i.e., components that map the rich Graph outputs of the network to the final energy prediction. This facilitates the integration of user-defined long-range interaction models.

Furthermore, we introduce a mechanism for global charge conditioning in *mlip* v2, similar to those developed in UMA [9]. We observed that MLIP performance can degrade when modeling systems with varying global charge (see Appendix C), as differences in formation energies across charge states introduce additional complexity. Incorporating total charge information can therefore improve predictive accuracy in such settings. *mlip* v2 enables this by adding an embedding of the total system charge, which complements the standard atomic number embedding. Both embeddings are concatenated and passed through a lightweight MLP to produce part of the initial model features.

5.2 Training with Hessian labels

Second-order derivatives of the energy with respect to positions are essential predictions in many downstream tasks, either explicitly (e.g., vibrational frequencies or zero point energy) or implicitly via running Hessian estimates (e.g., geometry relaxation with BFGS [47–49] or transition state search with the dimer method [50]). Incorporating higher-order derivatives of the energy with respect to atomic coordinates during the training has therefore gained a lot of interest recently, with various approaches being developed, either via automatic differentiation [51, 52] or direct Hessian prediction [53]. While forces define the slope of the Potential Energy Surface (PES), second-order derivatives carry broader curvature information around each training geometry, further highlighting and differentiating local minima, maxima, saddle points or inflections. This additional information has motivated the use of subsampled Hessian rows during training as a distillation strategy for large foundation models [54], an approach adopted in *mlip* v2.

Predicting the full Hessian matrix \mathbf{H} for each graph in a batch, and then backpropagating their variations with respect to parameters during training would be prohibitively computationally expensive. Differentiating all forces F_i with respect to all atomic coordinates r_i scales quadratically with respect to system size,

$$\mathbf{H}_{ij} = \frac{\partial^2 E}{\partial \mathbf{r}_i \partial \mathbf{r}_j} = -\frac{\partial \mathbf{F}_i}{\partial \mathbf{r}_j} \quad . \quad (3)$$

To address this limitation, several works in the literature have explored computing Hessian rows via Vector-Jacobian Products (VJP) and Hessian-Vector Products (HVP), as an alternative to directly learning the full Hessian [52, 54].

During training, *mlip* follows the approach of [54] by differentiating only selected force components $\mathbf{F}^{(S)}$ with respect to all atomic coordinates. For each graph g in the batch, and every row index $\rho = 1 \dots R$, the subsampling consists of a node index $i_{\rho,g}$ chosen within g , and force predictions on the indices $i_{\rho,g} \in \mathcal{S}$ are summed over distinct graphs of the batch. Reverse-mode automatic differentiation (VJP) on these predictions then effectively yields a matrix of size $R \times 3n$, where n is the total number of nodes,

$$\mathbf{H}_{\rho j}^{(S)} = -\frac{\partial \mathbf{F}_{\rho}^{(S)}}{\partial \mathbf{r}_j} \quad \text{where} \quad \mathbf{F}_{\rho}(\mathbf{r}) = \sum_{g \in \text{graphs}} \mathbf{F}_{i_{\rho,g}} \quad . \quad (4)$$

Since distinct graphs do not interact, each row \mathbf{H}_{ρ} is the concatenation of Hessian rows coming from different graphs g in the batch, which is how the Hessian labels are preprocessed in practice. This

sampling-based approximation makes it feasible to include larger and more diverse systems in the training process, thereby broadening the range of accessible reaction types and chemical elements.

The *mlip* v2 library includes the necessary data handling components to efficiently work with Hessian-based training signals in a batched setting. The modularity of its data processing pipeline allows to seamlessly hook into both the system pre-processing stage (padding full Hessian matrices to a common width) and the graph post-processing stage (subsample distinct indices at each epoch, forward them to the final prediction stage via the Graph object). Note that in addition to subsampled Hessian training, we also support full Hessian matrix inference. For validation, we present a brief study to assess the correctness of our Hessian label training approach in Appendix B.

5.3 Multi-head fine-tuning

MLIPs pretrained on large and chemically diverse datasets can be specialized to downstream applications through fine-tuning, for example, to a specific chemistry, level of theory or property of interest. A central challenge in this setting is reconciling the often incompatible labeling conventions across datasets, such as different DFT functionals, basis sets or label availability, while avoiding catastrophic forgetting of the original training distribution. Building on multi-head fine-tuning approaches, introduced for MLIPs in [28, 55], *mlip* v2 introduces a unified multi-head fine-tuning framework that addresses both points and is agnostic to the model architecture.

The framework is built on two design choices: a shared equivariant backbone paired with per-dataset readout heads, and a single implementation reused across all model architectures. For a graph g originating from dataset $d_g \in \{1, \dots, D\}$, the predicted total energy is given by

$$\tilde{E}_g = \sum_{i \in g} \left[\mathcal{R}_{d_g}(h_i) + E_0^{(d_g)}(z_i) \right] \quad (5)$$

where $h_i \in \mathbb{R}^F$ is the latent feature of atom i produced by the shared backbone, \mathcal{R}_d is the readout for dataset d , and $E_0^{(d)}$ is the dataset-specific table of reference atomic energies indexed by atomic number z_i . The same mechanism is reused across all supported architectures (MACE, NequIP, ViSNet, and eSEN), so extending a model with an additional head requires no architecture-specific code.

To mitigate catastrophic forgetting during fine-tuning, examples from the pre-training dataset are replayed along the new dataset(s) [55], and each additional dataset receives its own readout head and atomic-energy table. Datasets in practice may carry heterogeneous label sets, and hence batches are homogenized by filling missing entries with NaN sentinels, which are masked out of the loss.

At inference time, the active head is selected by dataset name or index, optionally combined with graph-level conditions that are charge and spin multiplicity, pinning the model to the corresponding head. When using the Mixture-of-Experts formalism with eSEN, the routed expert kernels can be further contracted into a single dense kernel, recovering the runtime cost of a standard single-head model. The corresponding API is detailed in Appendix A.

5.4 Transition state search

Locating the transition state of chemical reactions is an important task in many workflows utilizing MLIPs to model chemical reactivity. *mlip* v2 includes a custom engine with an interface to the nudged elastic band (NEB) method implemented in ASE ⁴.

In the NEB method [56], a set of interpolated structures, called images, between reactant and product structures of the reaction is created. Adjacent images are linked by a harmonic spring potential. The geometry of the linked images \mathbf{R}_i is then optimized considering the spring forces between images $\mathbf{F}_{i,\parallel}^S$ and the actual physical forces perpendicular to the band of images $\nabla E(\mathbf{R}_{i,\perp})$,

$$\mathbf{F}_i = \mathbf{F}_{i,\parallel}^S - \nabla E(\mathbf{R}_{i,\perp}) \quad . \quad (6)$$

⁴<https://ase-lib.org>

After optimizing the geometry to minimize F_i , the image with the highest potential energy can be selected as transition state guess. A useful modification is the climbing image variant of NEB [57]. Here, the spring forces for the image highest in potential energy are removed, and the physical forces along the band are inverted, driving the image upwards in energy along the band to find the transition state. This variant should only be applied to a band that has already been optimized to some extent.

The NEB engine in *mlip* v2 allows the user to define the number of images and the force constant between images. The NEB workflow can be started with only the structures of reactants and products, or a transition state guess can be provided as well. Prior to geometry optimization of the band, interpolation between the provided structures is done using the image dependent pair potential (IDPP) method [58]. The NEB engine also allows providing more than three images to define an entire band, which will be optimized without interpolation. This option is especially useful for subsequent NEB simulations, for instance, using the climbing image variant.

5.5 NPT ensemble simulations

The isothermal-isobaric (NPT) ensemble, in which the number of particles N , pressure P , and temperature T are held constant, is commonly used for simulating condensed-phase systems under realistic thermodynamic conditions. In contrast to the NVT ensemble, NPT simulations allow the simulation cell to fluctuate such that the system equilibrates to a target pressure, making it particularly important for studies of solvation, phase behavior, and biomolecular systems in explicit solvent.

mlip v2 introduces support for NPT simulations through a JAX-based implementation of the Monte Carlo (MC) barostat [59, 60], following the design of the OpenMM reference implementation [61]. This barostat is well-suited to MLIPs, as it performs periodic volume update proposals that are accepted or rejected using a Metropolis criterion based only on the change in potential energy and a $P\Delta V$ work term, avoiding the expensive stress evaluations required by other common barostats such as Berendsen [62] or Parrinello-Rahman [63]. When combined with the Langevin integrator already supported for NVT simulations, this enables NPT sampling across both the ASE and JAX-MD backends. While coupling a Monte Carlo barostat with Langevin dynamics can raise questions regarding thermodynamic consistency, stochastic collisions from the Langevin heat bath and the Metropolis-Hastings criterion work together to preserve detailed balance and ensure correct statistical sampling of the phase space [64]. Our implementation also supports batched simulations, in which multiple systems with independent cells and random seeds evolve in parallel on a single device. For validation of our implementation, see Appendix D.

6 Dataset and pre-trained models

Along with the updated version of the library, we provide pre-trained models compatible with the updated model implementations. These models are released on HuggingFace⁵ under a non-commercial license. The models were trained on a curated version of the SPICE2 subset of OMOL25 [65] consisting of 1,763,962 structures. In Appendix E, we describe dataset cleaning, splitting strategy, and training details. The full details of the model and training hyperparameters can be found in Appendix F.

In Figure 2, we present the validation of the four pre-trained models, MACE, NequIP and VisNet, and eSEN. Each model was assessed with two standard error metrics: the mean absolute error (MAE) in predicted energies per atom (meV/atom) and the MAE in atomic forces (meV/Å). Validation was conducted across seven subsets of SPICE2, comprising 172,838 structures in total. In Appendix H, we present additional error metrics for these models, including root-mean-squared error (RMSE) and errors for atomic partial charge prediction (MAE and RMSE). eSEN achieves the lowest energy and force errors for most subsets, while the other models exhibit very similar errors. Across most models, significantly higher energy errors are observed in the DES370K subset than in the other subset, and similarly, we obtain higher force errors in the solvated PubChem subset. As can be seen

⁵<https://huggingface.co/collections/InstaDeepAI/ml-interatomic-potentials>

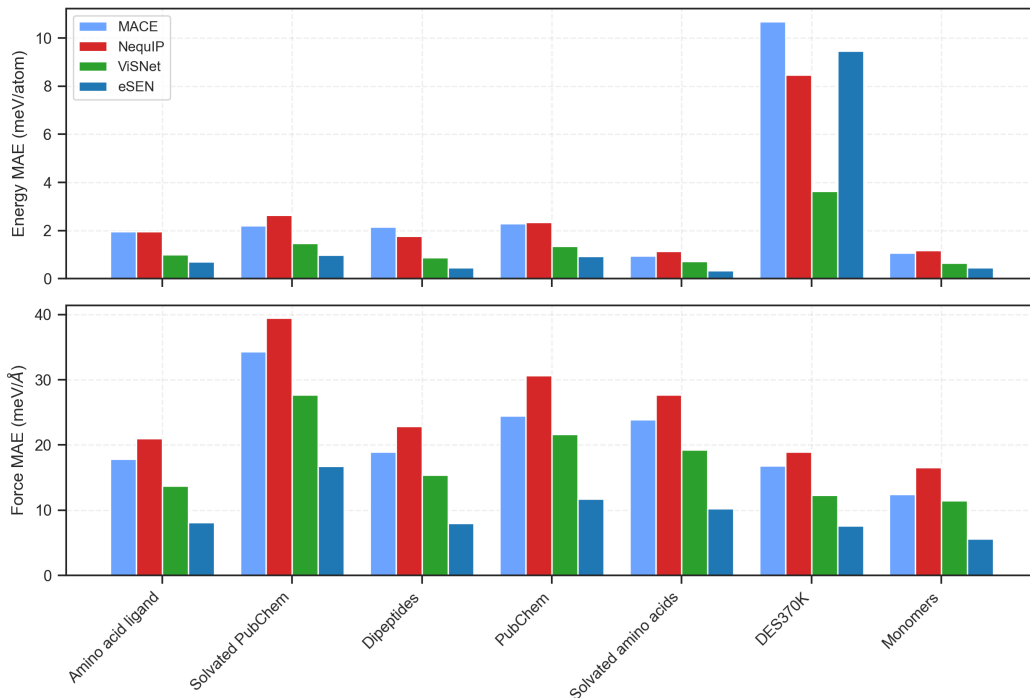


Figure 2: Validation set mean absolute errors (MAE) for energy per atom (meV/atom) and atomic forces (meV/Å) across seven molecular subsets in the SPICE2 subset of the OMOL25 dataset. The four pre-trained models MACE, NequIP, ViSNet, and eSEN are evaluated. The subsets include: amino acid ligands, solvated PubChem, dipeptides, PubChem, solvated amino acids, DES370K and monomers. MAE values reflect the deviation from DFT reference calculations. We emphasize that these results are intended to be indicative of the performance achievable with the library rather than a direct benchmark between architectures, as comparable hyperparameter settings are difficult to define.

in Appendix H, partial charge predictions are accurate across all subsets with only slightly higher errors observed for MACE and the DES370K subset. Furthermore, it should be noted that while validation errors are relevant metrics to measure training performance, they are not sufficient to attest to a model’s ability to simulate correct physics [6]. Finally, we also present runtime metrics for each of the four pre-trained models in Appendix H (see Table 7).

7 Pre-trained models assessment by MLIPAudit

To validate our new architectural features and the integration of data derived from the OMOL25 [65] dataset, we evaluate our pre-trained models across the standardized suite of benchmarks provided by MLIPAudit [6]. Because the primary focus of this work is to showcase the library’s novel software features and implementations, this section serves as a validation check to ensure downstream consistency and physical fidelity, with comprehensive analysis deferred to the Appendix.

All four architectures, eSEN, ViSNet, MACE, and NequIP, achieve perfect or near-perfect scores on bond length distributions, ring planarity, and reference geometry stability, and strong scores on conformer selection (0.88–0.95) and long-timescale structural stability (≈ 0.90), confirming physical fidelity across the model family. eSEN achieves the highest overall score (0.716), followed by ViSNet (0.699). MACE and NequIP score similarly ≈ 0.67 , in line with the obtained scores by the pre-trained models release with the v1 version of this library [1]. Per-benchmark scores for all models are reported in the Appendix G.

8 Conclusion and outlook into future development

In summary, *mip* v2 provides a unified, scalable, and extensible framework that significantly advances the practical applicability of MLIPs for complex molecular simulations. We are committed to maintaining the library as an open-source, actively developed project, ensuring its long-term reliability, usability, and continued alignment with advances in both machine learning and atomistic simulation. Looking ahead, we are already working on deploying additional capabilities in the near future, in particular:

- Deploying MoE formalism to all implemented architectures.
- Including additional alternative tensor product layers such as Vector Spherical Tensor Products [33–36].
- Including transformer-based MLIP architectures as some are becoming competitive in terms of runtime-accuracy trade off [40, 66].
- Deploying functionalities for better treatment of electrostatics and long range interactions, e.g. similar to MACE-POLAR [32].

Acknowledgments

This work was supported by Cloud TPUs from Google’s TPU Research Cloud (TRC). We would also like to thank Bohan Cao from Nankai University / Zhongguancun Academy for the numerous suggestions and conversations.

References

- [1] Christoph Brunken, Olivier Peltre, Heloise Chomet, Lucien Walewski, Manus McAuliffe, Valentin Heyraud, Solal Attias, Martin Maarand, Yessine Khanfir, Edan Toledo, Fabio Falcioni, Marie Bluntzer, Silvia Acosta-Gutiérrez, and Jules Tilly. Machine learning interatomic potentials: library for efficient training, model development and simulation of molecular systems, 2025. URL <https://arxiv.org/abs/2505.22397>.
- [2] Samuel S. Schoenholz and Ekin D. Cubuk. Jax, m.d.: A framework for differentiable physics, 2020. URL <https://arxiv.org/abs/1912.04232>.
- [3] Maitreyee Sharma Priyadarshini and Connor Ganley. Diversity-driven training of machine-learned force fields. In *AI for Accelerated Materials Design - NeurIPS 2025*, 2025. URL <https://openreview.net/forum?id=wNuR048JSn>.
- [4] Taoyong Cui, Zihan Wang, and Tong Wang. Enhancing non-local interaction modeling for ab initio biomolecular calculations and simulations with visnet-pima. *bioRxiv*, 2026. doi: 10.64898/2026.03.18.712561. URL <https://www.biorxiv.org/content/early/2026/03/20/2026.03.18.712561>.
- [5] Xu Huang, Junwu Chen, Philippe Schwaller, and Gerbrand Ceder. Skillpuzzler: A self-evolving agentic framework for materials and chemistry research with minimal reliance on predefined tools. In *NeurIPS 2025 AI for Science Workshop*, 2025. URL <https://openreview.net/forum?id=Mc1JTnKQIH>.
- [6] Leon Wehrhan, Lucien Walewski, Marie Bluntzer, Heloise Chomet, Jules Tilly, Christoph Brunken, and Silvia Acosta-Gutiérrez. Mlipaudit: A benchmarking tool for machine learned interatomic potentials, 2025. URL <https://arxiv.org/abs/2511.20487>.
- [7] Saro Passaro and C. Lawrence Zitnick. Reducing so(3) convolutions to so(2) for efficient equivariant gnns. In *Proceedings of the 40th International Conference on Machine Learning, ICML'23*. JMLR.org, 2023.
- [8] Xiang Fu, Brandon M. Wood, Luis Barroso-Luque, Daniel S. Levine, Meng Gao, Misko Dzamba, and C. Lawrence Zitnick. Learning smooth and expressive interatomic potentials for physical property prediction, 2025. URL <https://arxiv.org/abs/2502.12147>.
- [9] Brandon M. Wood, Misko Dzamba, Xiang Fu, Meng Gao, Muhammed Shuaibi, Luis Barroso-Luque, Kareem Abdelmaqsood, Vahe Gharakhanyan, John R. Kitchin, Daniel S. Levine, Kyle Michel, Anuroop Sriram, Taco Cohen, Abhishek Das, Ammar Rizvi, Sushree Jagriti Sahoo, Zachary W. Ulissi, and C. Lawrence Zitnick. Uma: A family of universal models for atoms, 2026. URL <https://arxiv.org/abs/2506.23971>.
- [10] Simon Batzner, Albert Musaelian, Lixin Sun, Mario Geiger, Jonathan P. Mailoa, Mordechai Kornbluth, Nicola Molinari, Tess E. Smidt, and Boris Kozinsky. E(3)-equivariant graph neural networks for data-efficient and accurate interatomic potentials. *Nature Communications*, 13(1), May 2022. ISSN 2041-1723. doi: 10.1038/s41467-022-29939-5. URL <http://dx.doi.org/10.1038/s41467-022-29939-5>.
- [11] Johann Brehmer, Sönke Behrends, Pim de Haan, and Taco Cohen. Does equivariance matter at scale?, 2024. URL <https://arxiv.org/abs/2410.23179>.
- [12] K. T. Schütt, H. E. Sauceda, P.-J. Kindermans, A. Tkatchenko, and K.-R. Müller. Schnet – a deep learning architecture for molecules and materials. *The Journal of Chemical Physics*, 148 (24), March 2018. ISSN 1089-7690. doi: 10.1063/1.5019779. URL <http://dx.doi.org/10.1063/1.5019779>.

- [13] Kristof T. Schütt, Pan Kessel, Michael Gastegger, Kim A. Nicoli, Alexandre Tkatchenko, and Klaus-Robert Müller. SchNetPack: A Deep Learning Toolbox For Atomistic Systems. *Journal of Chemical Theory and Computation*, 15(1):448–455, 2019. doi: 10.1021/acs.jctc.8b00908. URL <https://doi.org/10.1021/acs.jctc.8b00908>.
- [14] Kristof T. Schütt, Stefaan S. P. Hessmann, Niklas W. A. Gebauer, Jonas Lederer, and Michael Gastegger. SchNetPack 2.0: A neural network toolbox for atomistic machine learning. *The Journal of Chemical Physics*, 158(14):144801, 04 2023. ISSN 0021-9606. doi: 10.1063/5.0138367. URL <https://doi.org/10.1063/5.0138367>.
- [15] Dylan M. Anstine, Roman Zubatyuk, and Olexandr Isayev. Aimnet2: a neural network potential to meet your neutral, charged, organic, and elemental-organic needs. *Chemical Science*, 2025. ISSN 2041-6539. doi: 10.1039/d4sc08572h. URL <http://dx.doi.org/10.1039/D4SC08572H>.
- [16] Tian Xie and Jeffrey C. Grossman. Crystal graph convolutional neural networks for an accurate and interpretable prediction of material properties. *Physical Review Letters*, 120(14), April 2018. ISSN 1079-7114. doi: 10.1103/physrevlett.120.145301. URL <http://dx.doi.org/10.1103/PhysRevLett.120.145301>.
- [17] Victor Garcia Satorras, Emiel Hooeboom, and Max Welling. E(n) equivariant graph neural networks, 2022. URL <https://arxiv.org/abs/2102.09844>.
- [18] Johannes Gasteiger, Janek Groß, and Stephan Günnemann. Directional message passing for molecular graphs. In *International Conference on Learning Representations (ICLR)*, 2020.
- [19] Johannes Gasteiger, Shankari Giri, Johannes T. Margraf, and Stephan Günnemann. Fast and uncertainty-aware directional message passing for non-equilibrium molecules. In *Machine Learning for Molecules Workshop, NeurIPS*, 2020.
- [20] Johannes Gasteiger, Florian Becker, and Stephan Günnemann. Gemnet: Universal directional graph neural networks for molecules. In M. Ranzato, A. Beygelzimer, Y. Dauphin, P.S. Liang, and J. Wortman Vaughan, editors, *Advances in Neural Information Processing Systems*, volume 34, pages 6790–6802. Curran Associates, Inc., 2021. URL https://proceedings.neurips.cc/paper_files/paper/2021/file/35cf8659cfc13224cbd47863a34fc58-Paper.pdf.
- [21] Johannes Gasteiger, Florian Becker, and Stephan Günnemann. Gemnet: Universal directional graph neural networks for molecules, 2024. URL <https://arxiv.org/abs/2106.08903>.
- [22] Yusong Wang, Tong Wang, Shaoning Li, Xinheng He, Mingyu Li, Zun Wang, Nanning Zheng, Bin Shao, and Tie-Yan Liu. Enhancing geometric representations for molecules with equivariant vector-scalar interactive message passing. *Nature Communications*, 15(1), January 2024. ISSN 2041-1723. doi: 10.1038/s41467-023-43720-2. URL <http://dx.doi.org/10.1038/s41467-023-43720-2>.
- [23] Tong Wang, Xinheng He, Mingyu Li, Yatao Li, Ran Bi, Yusong Wang, Chaoran Cheng, Xiangzhen Shen, Jiawei Meng, He Zhang, Haiguang Liu, Zun Wang, Shaoning Li, Bin Shao, and Tie-Yan Liu. Ab initio characterization of protein molecular dynamics with ai2bmd. *Nature*, 635(8040):1019–1027, November 2024. ISSN 1476-4687. doi: 10.1038/s41586-024-08127-z. URL <http://dx.doi.org/10.1038/s41586-024-08127-z>.
- [24] Maurice Weiler, Mario Geiger, Max Welling, Wouter Boomsma, and Taco Cohen. 3d steerable cnns: Learning rotationally equivariant features in volumetric data, 2018. URL <https://arxiv.org/abs/1807.02547>.
- [25] Risi Kondor, Zhen Lin, and Shubhendu Trivedi. Clebsch-gordan nets: a fully fourier space spherical convolutional neural network, 2018. URL <https://arxiv.org/abs/1806.09231>.

- [26] Ilyes Batatia, Simon Batzner, Dávid Péter Kovács, Albert Musaelian, Gregor N. C. Simm, Ralf Drautz, Christoph Ortner, Boris Kozinsky, and Gábor Csányi. The design space of $e(3)$ -equivariant atom-centered interatomic potentials, 2022. URL <https://arxiv.org/abs/2205.06643>.
- [27] Nathaniel Thomas, Tess Smidt, Steven Kearnes, Lusann Yang, Li Li, Kai Kohlhoff, and Patrick Riley. Tensor field networks: Rotation- and translation-equivariant neural networks for 3d point clouds, 2018. URL <https://arxiv.org/abs/1802.08219>.
- [28] Ilyes Batatia, Dávid Péter Kovács, Gregor N. C. Simm, Christoph Ortner, and Gábor Csányi. Mace: Higher order equivariant message passing neural networks for fast and accurate force fields, 2023. URL <https://arxiv.org/abs/2206.07697>.
- [29] Dávid Péter Kovács, J. Harry Moore, Nicholas J. Browning, Ilyes Batatia, Joshua T. Horton, Yixuan Pu, Venkat Kapil, William C. Witt, Ioan-Bogdan Magdău, Daniel J. Cole, and Gábor Csányi. Mace-off: Short-range transferable machine learning force fields for organic molecules. *Journal of the American Chemical Society*, May 2025. ISSN 1520-5126. doi: 10.1021/jacs.4c07099. URL <http://dx.doi.org/10.1021/jacs.4c07099>.
- [30] Ilyes Batatia, Philipp Benner, Yuan Chiang, Alin M. Elena, Dávid P. Kovács, Janosh Riebesell, Xavier R. Advincula, Mark Asta, Matthew Avaylon, William J. Baldwin, Fabian Berger, Noam Bernstein, Arghya Bhowmik, Samuel M. Blau, Vlad Cărare, James P. Darby, Sandip De, Flaviano Della Pia, Volker L. Deringer, Rokas Elijošius, Zakariya El-Machachi, Fabio Falcioni, Edvin Fako, Andrea C. Ferrari, Annalena Genreith-Schriever, Janine George, Rhys E. A. Goodall, Clare P. Grey, Petr Grigorev, Shuang Han, Will Handley, Hendrik H. Heenen, Kersti Hermansson, Christian Holm, Jad Jaafar, Stephan Hofmann, Konstantin S. Jakob, Hyunwook Jung, Venkat Kapil, Aaron D. Kaplan, Nima Karimitari, James R. Kermode, Namu Kroupa, Jolla Kullgren, Matthew C. Kuner, Domantas Kuryla, Guoda Liepuoniute, Johannes T. Margraf, Ioan-Bogdan Magdău, Angelos Michaelides, J. Harry Moore, Aakash A. Naik, Samuel P. Niblett, Sam Walton Norwood, Niamh O’Neill, Christoph Ortner, Kristin A. Persson, Karsten Reuter, Andrew S. Rosen, Lars L. Schaaf, Christoph Schran, Benjamin X. Shi, Eric Sivonxay, Tamás K. Stenczel, Viktor Svahn, Christopher Sutton, Thomas D. Swinburne, Jules Tilly, Cas van der Oord, Eszter Varga-Umbrich, Tejs Vegge, Martin Vondrák, Yangshuai Wang, William C. Witt, Fabian Zills, and Gábor Csányi. A foundation model for atomistic materials chemistry, 2024. URL <https://arxiv.org/abs/2401.00096>.
- [31] Dávid Péter Kovács, Ilyes Batatia, Eszter Sára Arany, and Gábor Csányi. Evaluation of the mace force field architecture: From medicinal chemistry to materials science. *The Journal of Chemical Physics*, 159(4), July 2023. ISSN 1089-7690. doi: 10.1063/5.0155322. URL <http://dx.doi.org/10.1063/5.0155322>.
- [32] Ilyes Batatia, William J. Baldwin, Domantas Kuryla, Joseph Hart, Elliott Kesoar, Alin M. Elena, Harry Moore, Mikołaj J. Gawkowski, Benjamin X. Shi, Venkat Kapil, Panagiotis Kourtis, Ioan-Bogdan Magdău, and Gábor Csányi. Mace-polar-1: A polarisable electrostatic foundation model for molecular chemistry, 2026. URL <https://arxiv.org/abs/2602.19411>.
- [33] Shengjie Luo, Tianlang Chen, and Aditi S. Krishnapriyan. Enabling efficient equivariant operations in the fourier basis via gaunt tensor products, 2024. URL <https://arxiv.org/abs/2401.10216>.
- [34] YuQing Xie, Ameya Daigavane, Mit Kotak, and Tess Smidt. The price of freedom: Exploring expressivity and runtime tradeoffs in equivariant tensor products. In *Forty-second International Conference on Machine Learning*, 2025. URL <https://openreview.net/forum?id=EvIwwGYTLc>.
- [35] YuQing Xie, Ameya Daigavane, Mit Kotak, and Tess Smidt. Asymptotically fast clebsch-gordan tensor products with vector spherical harmonics, 2026. URL <https://arxiv.org/abs/2602.21466>.

- [36] Valentin Heyraud, Zachary Weller-Davies, and Jules Tilly. Integral formulas for vector spherical tensor products, 2026. URL <https://arxiv.org/abs/2603.08630>.
- [37] Yi-Lun Liao and Tess Smidt. Equiformer: Equivariant graph attention transformer for 3d atomistic graphs. In *The Eleventh International Conference on Learning Representations*, 2023. URL <https://openreview.net/forum?id=KwmPfARg0TD>.
- [38] Yi-Lun Liao, Brandon M Wood, Abhishek Das, and Tess Smidt. Equiformerv2: Improved equivariant transformer for scaling to higher-degree representations. In *The Twelfth International Conference on Learning Representations*, 2024. URL <https://openreview.net/forum?id=mCOBKZmrzD>.
- [39] Yunyang Li, Lin Huang, Zhihao Ding, Xinran Wei, Chu Wang, Han Yang, Zun Wang, Chang Liu, Yu Shi, Peiran Jin, Tao Qin, Mark Gerstein, and Jia Zhang. E2former: An efficient and equivariant transformer with linear-scaling tensor products. In *The Thirty-ninth Annual Conference on Neural Information Processing Systems*, 2026. URL <https://openreview.net/forum?id=ls5L4IMEwt>.
- [40] Lin Huang, Chengxiang Huang, Ziang Wang, Yiyue Du, Chu Wang, Haocheng Lu, Yunyang Li, Xiaoli Liu, Arthur Jiang, and Jia Zhang. E2former-v2: On-the-fly equivariant attention with linear activation memory, 2026. URL <https://arxiv.org/abs/2601.16622>.
- [41] Eric Qu, Brandon M. Wood, Aditi S. Krishnapriyan, and Zachary W. Ulissi. A recipe for scalable attention-based mlips: unlocking long-range accuracy with all-to-all node attention, 2026. URL <https://arxiv.org/abs/2603.06567>.
- [42] Ahmed A. Elhag, Arun Raja, Alex Morehead, Samuel M. Blau, Hongtao Zhao, Christian Tyrchan, Eva Nittinger, Garrett M. Morris, and Michael M. Bronstein. Learning inter-atomic potentials without explicit equivariance, 2026. URL <https://arxiv.org/abs/2510.00027>.
- [43] Jonathan Godwin, Thomas Keck, Peter Battaglia, Victor Bapst, Thomas Kipf, Yujia Li, Kimberly Stachenfeld, Petar Veličković, and Alvaro Sanchez-Gonzalez. Jraph: A library for graph neural networks in jax., 2020. URL <http://github.com/deepmind/jraph>.
- [44] Oliver T. Unke and Markus Meuwly. Physnet: A neural network for predicting energies, forces, dipole moments and partial charges. *Journal of Chemical Theory and Computation*, 15(6): 3678–3693, 2019. doi: 10.1021/acs.jctc.9b00181.
- [45] Christoph Brunken, Sebastien Boyer, Mustafa Omar, Bakary N’tji Diallo, Karim Beguir, Nicolas Lopez Carranza, and Oliver Bent. Machine learning of force fields towards molecular dynamics simulations of proteins at DFT accuracy. In *ICLR 2024 Workshop on Geometry-grounded Graph Machine Learning (GEM)*, 2024. URL <https://openreview.net/forum?id=3Yjc10DCyq>.
- [46] Dylan Anstine, Roman Zubatyuk, and Olexandr Isayev. Aimnet2: a neural network potential to meet your neutral, charged, organic, and elemental-organic needs. *Chemical Science*, 16:10228, 2025. doi: 10.1039/D4SC08572H.
- [47] Roger Fletcher. A new approach to variable metric algorithms. *The Computer Journal*, 13(3): 317–322, 1970.
- [48] Donald Goldfarb. A family of variable metric updates derived by variational means. *Mathematics of Computation*, 24(109):23–26, 1970.
- [49] David F Shanno. Conditioning of quasi-newton methods for function minimization. *Mathematics of Computation*, 24(111):647–656, 1970.
- [50] Graeme Henkelman and Hannes Jónsson. A dimer method for finding saddle points on high dimensional potential surfaces using only first derivatives. *The Journal of Chemical Physics*, 111(15):7010–7022, 1999. doi: 10.1063/1.480097.

- [51] Austin Rodriguez, Justin S Smith, and Jose L Mendoza-Cortes. Does hessian data improve the performance of machine learning potentials? *Journal of Chemical Theory and Computation*, 21 (14):6698–6710, 2025.
- [52] Austin Rodriguez, Justin S Smith, Sakib Matin, Nicholas Lubbers, Kipton Barros, and Jose L Mendoza-Cortes. Projected hessian learning: Fast curvature supervision for accurate machine-learning interatomic potentials. *arXiv preprint arXiv:2603.04523*, 2026.
- [53] Andreas Burger, Luca Thiede, Nikolaj Rønne, Varinia Bernales, Nandita Vijaykumar, Tejs Vegge, Arghya Bhowmik, and Alán Aspuru-Guzik. Shoot from the hip: Hessian interatomic potentials without derivatives, 2025. URL <https://arxiv.org/abs/2509.21624>.
- [54] Ishan Amin, Sanjeev Raja, and Aditi Krishnapriyan. Towards fast, specialized machine learning force fields: Distilling foundation models via energy Hessians. *arXiv 2025*, doi: 10.48550. *arXiv preprint arXiv:2501.09009*, 2025.
- [55] Ilyes Batatia, Chen Lin, Joseph Hart, Elliott Kasoar, Alin M. Elena, Sam Walton Norwood, Thomas Wolf, and Gábor Csányi. Cross learning between electronic structure theories for unifying molecular, surface, and inorganic crystal foundation force fields, 10 2025. URL <https://arxiv.org/pdf/2510.25380>.
- [56] Graeme Henkelman and Hannes Jónsson. Improved tangent estimate in the nudged elastic band method for finding minimum energy paths and saddle points. *The Journal of Chemical Physics*, 113(22):9978–9985, 12 2000. ISSN 0021-9606. doi: 10.1063/1.1323224. URL <https://doi.org/10.1063/1.1323224>.
- [57] Graeme Henkelman, Blas P. Uberuaga, and Hannes Jónsson. A climbing image nudged elastic band method for finding saddle points and minimum energy paths. *The Journal of Chemical Physics*, 113(22):9901–9904, 12 2000. ISSN 0021-9606. doi: 10.1063/1.1329672. URL <https://doi.org/10.1063/1.1329672>.
- [58] Søren Smidstrup, Andreas Pedersen, Kurt Stokbro, and Hannes Jónsson. Improved initial guess for minimum energy path calculations. *The Journal of Chemical Physics*, 140(21):214106, 06 2014. ISSN 0021-9606. doi: 10.1063/1.4878664. URL <https://doi.org/10.1063/1.4878664>.
- [59] Kim-Hung Chow and David M. Ferguson. Isothermal-isobaric molecular dynamics simulations with monte carlo volume sampling. *Computer Physics Communications*, 91(1):283–289, 1995. ISSN 0010-4655. doi: [https://doi.org/10.1016/0010-4655\(95\)00059-O](https://doi.org/10.1016/0010-4655(95)00059-O). URL <https://www.sciencedirect.com/science/article/pii/0010465595000590>.
- [60] Johan Åqvist, Petra Wennerström, Martin Nervall, Sinisa Bjelic, and Bjørn O. Brandsdal. Molecular dynamics simulations of water and biomolecules with a monte carlo constant pressure algorithm. *Chemical Physics Letters*, 384(4):288–294, 2004. ISSN 0009-2614. doi: <https://doi.org/10.1016/j.cplett.2003.12.039>. URL <https://www.sciencedirect.com/science/article/pii/S0009261403021687>.
- [61] Peter Eastman, Jason Swails, John D. Chodera, Robert T. McGibbon, Yutong Zhao, Kyle A. Beauchamp, Lee-Ping Wang, Andrew C. Simmonett, Matthew P. Harrigan, Chaya D. Stern, Rafal P. Wiewiora, Bernard R. Brooks, and Vijay S. Pande. Openmm 7: Rapid development of high performance algorithms for molecular dynamics. *PLOS Computational Biology*, 13 (7):1–17, 07 2017. doi: 10.1371/journal.pcbi.1005659. URL <https://doi.org/10.1371/journal.pcbi.1005659>.
- [62] H. J. C. Berendsen, J. P. M. Postma, W. F. van Gunsteren, A. DiNola, and J. R. Haak. Molecular dynamics with coupling to an external bath. *The Journal of Chemical Physics*, 81(8):3684–3690, 1984. doi: 10.1063/1.448118.

- [63] M. Parrinello and A. Rahman. Polymorphic transitions in single crystals: A new molecular dynamics method. *Journal of Applied Physics*, 52(12):7182–7190, 1981. doi: 10.1063/1.328693.
- [64] Jiaming Liang, Siddharth Mitra, and Andre Wibisono. Characterizing dependence of samples along the langevin dynamics and algorithms via contraction of ϕ -mutual information. In *Proceedings of Thirty Eighth Conference on Learning Theory*, volume 291 of *Proceedings of Machine Learning Research*, pages 3730–3731. PMLR, 30 Jun–04 Jul 2025. URL <https://proceedings.mlr.press/v291/liang25b.html>.
- [65] Daniel S. Levine, Muhammed Shuaibi, Evan Walter Clark Spotte-Smith, Michael G. Taylor, Muhammad R. Hasyim, Kyle Michel, Ilyes Batatia, Gábor Csányi, Misko Dzamba, Peter Eastman, Nathan C. Frey, Xiang Fu, Vahe Gharakhanyan, Aditi S. Krishnapriyan, Joshua A. Rackers, Sanjeev Raja, Ammar Rizvi, Andrew S. Rosen, Zachary Ulissi, Santiago Vargas, C. Lawrence Zitnick, Samuel M. Blau, and Brandon M. Wood. The open molecules 2025 (omol25) dataset, evaluations, and models, 2025. URL <https://arxiv.org/abs/2505.08762>.
- [66] Yi-Lun Liao, Alexander J. Hoffman, Sabrina C. Shen, Alexandre Duval, Sam Walton Norwood, and Tess Smidt. Equiformerv3: Scaling efficient, expressive, and general se(3)-equivariant graph attention transformers, 2026. URL <https://arxiv.org/abs/2604.09130>.
- [67] Peter Eastman, Pavan Kumar Behara, David L. Dotson, Raimondas Galvelis, John E. Herr, Josh T. Horton, Yuezhi Mao, John D. Chodera, Benjamin P. Pritchard, Yuanqing Wang, Gianni De Fabritiis, and Thomas E. Markland. Spice, a dataset of drug-like molecules and peptides for training machine learning potentials. *Scientific Data*, 10, January 2023. doi: 10.1038/s41597-022-01882-6. URL <https://doi.org/10.1038/s41597-022-01882-6>.
- [68] Mathias Schreiner, Arghya Bhowmik, Tejs Vegge, Jonas Busk, and Ole Winther. Transition1x - a dataset for building generalizable reactive machine learning potentials. *Scientific Data*, 9(1), December 2022. ISSN 2052-4463. doi: 10.1038/s41597-022-01870-w. URL <http://dx.doi.org/10.1038/s41597-022-01870-w>.
- [69] Qiyuan Zhao, Sai Mahit Vaddadi, Michael Woulfe, Lawal A. Ogunfowora, Sanjay S. Garimella, Olexandr Isayev, and Brett M. Savoie. Comprehensive exploration of graphically defined reaction spaces. *Scientific Data*, 10(1), March 2023. ISSN 2052-4463. doi: 10.1038/s41597-023-02043-z. URL <http://dx.doi.org/10.1038/s41597-023-02043-z>.
- [70] Qiming Sun, Timothy C Berkelbach, Nick S Blunt, George H Booth, Sheng Guo, Zhendong Li, Junzi Liu, James D McClain, Elvira R Sayfutyarova, Sandeep Sharma, et al. Pyscf: the python-based simulations of chemistry framework. *Wiley Interdisciplinary Reviews: Computational Molecular Science*, 8(1):e1340, 2018.
- [71] Xiang Gao, Farhad Ramezanghorbani, Olexandr Isayev, Justin S Smith, and Adrian E Roitberg. Torchani: a free and open source pytorch-based deep learning implementation of the ani neural network potentials. *Journal of chemical information and modeling*, 60(7):3408–3415, 2020.
- [72] Mohammadamin Tavakoli, Ryan J. Miller, Mirana Claire Angel, Michael A. Pfeiffer, Eugene S. Gutman, Aaron D. Mood, David Van Vranken, and Pierre Baldi. Pmechdb: A public database of elementary polar reaction steps. *Journal of Chemical Information and Modeling*, 64:1975–1983, 2024. doi: 10.1021/acs.jcim.3c01810.
- [73] Simone Melchionna, Giovanni Ciccotti, and Brad Lee Holian. Hoover NPT dynamics for systems varying in shape and size. *Molecular Physics*, 78(3):533–544, 1993. doi: 10.1080/00268979300100371.
- [74] William L. Jorgensen, Jayaraman Chandrasekhar, Jeffrey D. Madura, Roger W. Impey, and Michael L. Klein. Comparison of simple potential functions for simulating liquid water. *The Journal of Chemical Physics*, 79(2):926–935, 1983. doi: 10.1063/1.445869. URL <https://doi.org/10.1063/1.445869>.

- [75] Carlos Vega and Jose L. F. Abascal. Simulating water with rigid non-polarizable models: a general perspective. *Physical Chemistry Chemical Physics*, 13(44):19663–19688, 2011. doi: 10.1039/c1cp22168j.
- [76] Mattia Bernetti and Giovanni Bussi. Pressure control using stochastic cell rescaling. *The Journal of Chemical Physics*, 153(11):114107, 2020. doi: 10.1063/5.0020514.
- [77] Alan K. Soper. The radial distribution functions of water and ice from 220 to 673 K and at pressures up to 400 MPa. *Chemical Physics*, 258(2–3):121–137, 2000. doi: 10.1016/S0301-0104(00)00179-8.

A Overview of API updates

The following contains an overview of the most essential API updates of *mlip* v2. For a more in-depth migration guide and all other details of how to use the *mlip* library in general and, more specifically, the new v2 features, we refer to the code documentation.⁶

The ChemicalSystem and Graph classes

As mentioned in the main text, we introduce the new Graph class to replace the former `graph.GraphsTuple`, which becomes the central data structure throughout all workflows. For an applied user interested in running standard training, inference, and simulation workflows, this change does not have a direct impact on their workflows. Furthermore, the already existing `ChemicalSystem` class was extended with a constructor from an `ase.Atoms` object, so that it becomes straightforward to perform inference on a single system, as demonstrated below.

```
import ase.io
from mlip.data import ChemicalSystem
from mlip.graph import Graph

# From molecular structure file to input graph
atoms = ase.io.read("/path/to/xyz/or/pdb/file")
chem_system = ChemicalSystem.from_ase_atoms(atoms)
graph = Graph.from_chemical_system(chem_system, graph_cutoff_angstrom=5.0)

# Generate prediction for input graph
force_field = _get_force_field_placeholder()
prediction = force_field(graph)

# Display energy prediction
print(prediction.energy)
```

Note that chemical system, graph, and prediction objects contain additional fields in v2 compared to v1 corresponding to the presented new features, e.g., partial charges or Hessian matrices. Instead of computing a Prediction object, the new method `ForceField.calculate` allows a user to compute an output Graph object directly. Internally, this output graph is transformed into a prediction via the `Graph.to_prediction` method when the force field is called on an input graph.

Dataset processing

The most significant breaking API update relates to the processing of a full dataset. In *mlip* v1, the classes `ChemicalSystemReader` and `GraphDatasetBuilder` operate on three dataset splits together, one for training, validation and test set. To generalize the dataset processing code towards single-dataset inference as well as multi-dataset training and fine-tuning use cases, in v2, (i) the `ChemicalSystemReader` operates on a single split only, (ii) a new `SingleGraphDatasetBuilder` class is introduced to generate the graphs for a single split, and (iii) the `GraphDatasetBuilder` receives an updated API that allows users to easily orchestrate multiple-split use cases, not limited to the standard training use case but also including multi-dataset scenarios. Below, we provide a code example for the standard training use case.

```
from mlip.data import ExtxyzReader, GraphDatasetBuilder, BuilderMode

readers = {
    "train": ExtxyzReader("/path/to/train.xyz"),
    "val": ExtxyzReader("/path/to/val.xyz"),
    "test": ExtxyzReader("/path/to/test.xyz"),
}
```

⁶<https://instadeepai.github.io/mlip>

```

builder_cfg = GraphDatasetBuilder.Config()
builder = GraphDatasetBuilder(
    readers,
    builder_cfg,
    BuilderMode.TRAINING,
    dataset_info=None, # compute from 'train' set
)

graph_datasets = builder.get_datasets()

# Access training set
train_set = graph_datasets["train"]

```

With this API, both multi-dataset training (e.g., for a Mixture-of-Experts eSEN model) and multi-head fine-tuning can be set up easily. For the former, a readers dictionary can be configured as follows:

```

readers = {
    "dataset_1": {"train": ..., "val": ...},
    "dataset_2": {"train": ..., "val": ...},
    "dataset_3": {"train": ..., "val": ...},
}

```

Dataset names can be chosen freely; the only reserved key is *train*, which denotes the training split for each dataset. For multi-head fine-tuning, the setup is largely identical, with the exception that one dataset must be named *replay*. This dataset represents replayed training data, from which the relevant statistics are extracted to construct the DatasetInfo object. Note that in both of these cases, the builder mode `BuilderMode.MULTI` should be passed to the `GraphDatasetBuilder` constructor.

Force field interface

As outlined in the main text, the classes derived from `MLIPNetwork`, which implement the core model architectures, now follow a unified `Graph` \rightarrow `Graph` call signature. This design significantly increases flexibility with respect to both model inputs and outputs, allowing arbitrary features to be consumed and produced within a consistent interface. While this change is particularly relevant for model developers and researchers extending the library with new architectures or capabilities, it remains largely transparent to most applied users.

For standard usage, the primary interface continues to be the `ForceField` class, which has undergone only minor changes in its overall usage. One notable addition, however, is the introduction of the `Property` abstraction. This concept is used both to define the set of properties a model can provide and to specify the properties required by a given `ForceField`. For instance, in addition to the default predictions of energies and forces, users can request further quantities such as Hessians or partial charges in a consistent and extensible manner. The new concept is demonstrated below.

```

from mlip.models import Mace, ForceField
from mlip.models.model_io import load_model_from_zip
from mlip.typing.properties import Properties

# Request additional properties
# Energy and forces are requested by default
req_properties = Properties(hessian=True, partial_charges=True)

# Load pre-trained model
force_field = load_model_from_zip(
    Mace, "/path/to/pretrained_model.zip", req_properties
)

```

```
# Predict
force_field, graph = _setup_placeholder()
prediction = force_field(graph)

# For example, display partial charges
print(prediction.partial_charges)
```

For Mixture-of-Experts models (currently supported for the eSEN architecture), it is often desirable to specialize the model for inference by selecting a single expert after training, in order to improve inference efficiency. In the v2 API, this can be done straightforwardly by providing an `InferenceContext` when loading the model. This context specifies the conditions under which the model should be specialized, including information such as the training dataset, charge, and spin multiplicity.

```
from mlip.models import Mace, ForceField
from mlip.models.model_io import load_model_from_zip
from mlip.models.inference_context import InferenceContext

# Specialize model for neutral systems without unpaired electrons
# and, for example, for the "spice" dataset
inference_context = InferenceContext(
    charge=0,
    spin_multiplicity=1,
    dataset_name="spice",
)

# Load pre-trained model
force_field = load_model_from_zip(
    Mace,
    "/path/to/pretrained_model.zip",
    inference_context=inference_context,
)
```

Note that the dataset name must match the key used during multi-dataset processing, as outlined above.

B Training on Hessian labels

This section provides a brief study on the effect of training MLIP models on Hessian labels to validate our approach presented in section 5.2 in the main text.

To enable a controlled and consistent evaluation of the proposed Hessian training strategy, including its implementation, inference procedure, and label processing, we constructed a dedicated dataset, including reaction data due to the relevance of accurate Hessian predictions for chemical reaction studies. The resulting dataset contains 451,000 geometries composed of four chemical elements (C, H, N, and O). It combines 116,000 systems sampled from the SPICE dataset [67], 126,000 from the synthetic reactive Transition1x dataset [68], and 209,000 from the Reaction Graph Depth 1 (RGD1) dataset [69]. Within these subsets, 16,000 and 26,000 Hessians were computed for systems from SPICE and Transition1x, respectively. In addition, 9,000 Hessians were calculated for reactants, products, and transition states corresponding to 3,000 reactions from the RGD1 dataset.

The Hessian reference calculations were carried out using the PySCF [70] software at the ω B97M-V/def2-TZVPD level of theory. The systems for which Hessians were evaluated span a range of molecular sizes, up to a maximum of 31 atoms. This upper bound was determined by the computational limits of the available hardware.

To ensure a fair and transparent comparison, we trained two identical MACE models using this dataset, configured as described in Table 4. The baseline model was trained using energy and force

losses only, while the second model additionally incorporates supervision from the available Hessian labels. Both models were trained for 220 epochs. In the Hessian-supervised setting, eight rows were randomly sampled from each graph in a batch for Hessian loss evaluation.

For runtime assessment, we perform energy and force inference on 999 systems drawn from 333 held-out reactions, with a maximum system size of 31 atoms. The Hessian-trained model is additionally used to predict full Hessian matrices for the same set of structures. For standard energy and force inference, the average computation time per structure is 0.35 seconds. When extending the inference to include full Hessian prediction, requiring differentiation of the force vectors with respect to all atomic positions, the average computation time increases to 0.89 seconds on a single NVIDIA H100 GPU.

To quantitatively assess the impact of Hessian supervision, we perform a statistical comparison of vibrational frequency predictions against DFT references. Table 1 reports the mean absolute errors (MAE) for a baseline MACE model and a model trained with Hessian labels. The evaluation is carried out separately for transition states and minimum-energy structures (reactants and products). The results show a clear and consistent reduction in error when Hessian information is included during training, demonstrating a significant improvement in the accuracy of MLIP-predicted vibrational frequencies.

To complement this aggregate analysis, we also provide a representative single-system comparison. Figure 3 illustrates the vibrational frequency spectrum for a transition state molecule from the RGD1 dataset (reaction ID: MR_127670_0, chemical formula: $C_2H_4N_8$, reactant: 1-methyl-2-(prop-1-en-2-yl)diazene, product: 2-diazobutane), showing that the spectrum predicted by the Hessian-trained MLIP is in closer agreement with the DFT reference, particularly in the high-frequency region. The vibrational frequencies ν_k are computed from the eigenvalues λ_k of the mass-weighted Hessian matrix using the TorchANI package [71].

Table 1: Mean absolute errors (MAE) for vibrational frequency predictions, comparing (i) a baseline MACE model and (ii) one trained with Hessian labels to the DFT reference. We distinguish between transition states and minimum-energy structures (reactants and products). We compute the shown metrics on 300 structures of each system type (hence, 600 in total) that are not in the training set. The results demonstrate that training on Hessian labels improves the accuracy of MLIP-predicted vibrational frequencies significantly.

Training strategy	Transition States	Reactants and Products
With Hessian labels	86.8 Hz	48.7 Hz
Baseline	253.9 Hz	82.9 Hz

C Impact of global charge embedding for training on charged systems

As mentioned in the main article, we found that MLIP models have low energy accuracy for globally charged systems. While this can be partially attributed to their sparse presence in training datasets, we demonstrate in this section that using total charge information for energy prediction significantly improves MLIP model performance, particularly on globally charged systems. The global charge information is fed into the model via a learned embedding that is concatenated with the atomic number embedding and routed through a small linear MLP, as is done in the UMA architecture [9]. The resulting latent vector is then used as input for the model’s message passing layers.

In this section, we present a brief study illustrating the potential benefits of incorporating a global charge embedding into any model. We trained two identical ViSNet models: one with the charge embedding and one without. To ensure that globally charged systems were well represented during training, we used a subsampled version of the PMechDB dataset [72] that displayed a high occurrence of charged systems. The models were trained on approximately 120,000 structures, containing roughly 40 % neutral molecules, 20 % negatively charged molecules, and 40 % positively charged molecules.

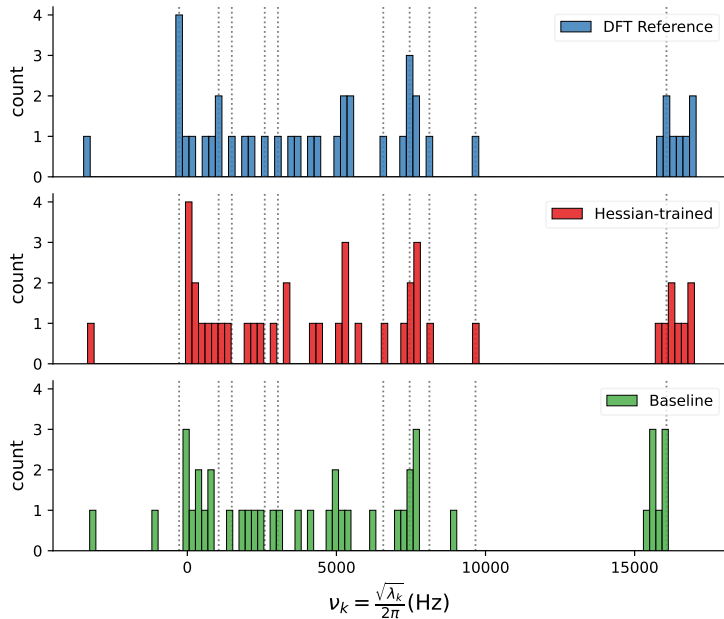


Figure 3: Comparison of vibrational frequencies computed with DFT, a MACE model trained on Hessian labels, and a baseline MACE model, for a single test system from the RGD1 dataset (reaction ID: MR_127670_0, chemical formula: $C_2H_4N_8$, reactant: 1-methyl-2-(prop-1-en-2-yl)diazene, product: 2-diazobutane). These results demonstrate the positive effect of the Hessian-supervised training on the alignment of the MACE predicted vibrational frequencies visually, compared to its baseline. For more statistically relevant averaged results on this dataset, see Table 1.

This experiment demonstrates that MLIP models’ ability to make accurate energy predictions is affected by the global charge of the systems to some extent. As shown in Figure 4, the model’s energy prediction improves significantly for highly charged systems. It is also evident that adding a global charge embedding improves the model’s accuracy for neutral systems. Note that the models in Figure 4 were trained on small datasets. This explains why the energy MAE of neutral systems is as high as 155 meV, compared to the much lower numbers presented in section 6 of the main text for our pre-trained models released alongside the library.

D Validation of JAX-based NPT integrators

To validate the NPT integrators included in this release, which use a JAX-based Monte Carlo (MC) barostat coupled to a Langevin thermostat, we compared thermodynamic observables from the JAX-MD and ASE implementations against two reference NPT methods available in the ASE package: *BerendsenNPT*, which combines a Berendsen [62] thermostat and barostat; and *MelchionnaNPT*, which combines Nosé–Hoover thermostat with Parrinello–Rahman barostat dynamics [73]. All four simulations used the pre-trained VisNet model on a system of 501 water molecules at 300 K and 1 atm. The system was minimised classically using the TIP3P force field [74] in OpenMM [61], after which production runs of 500ps were performed with the last 2/3 of each trajectory used for analysis.

The two JAX-based implementations show excellent agreement across all observables. Mean temperatures are consistent across all four methods (5 panel a), each running close to the 300 K target despite differences in thermostat algorithm. The isothermal compressibility κ_T , estimated from volume fluctuations via $\kappa_T = \langle \delta V^2 \rangle / (\langle V \rangle k_{BT})$, is in quantitative agreement between the ASE and JAX-MD MC barostats (5 panel b), with both lying above the experimental value of 0.452 GPa^{-1} [75], a known overestimation attributable to the force field rather than the barostat. The Berendsen barostat yields a markedly lower κ_T , consistent with its well-documented suppression of

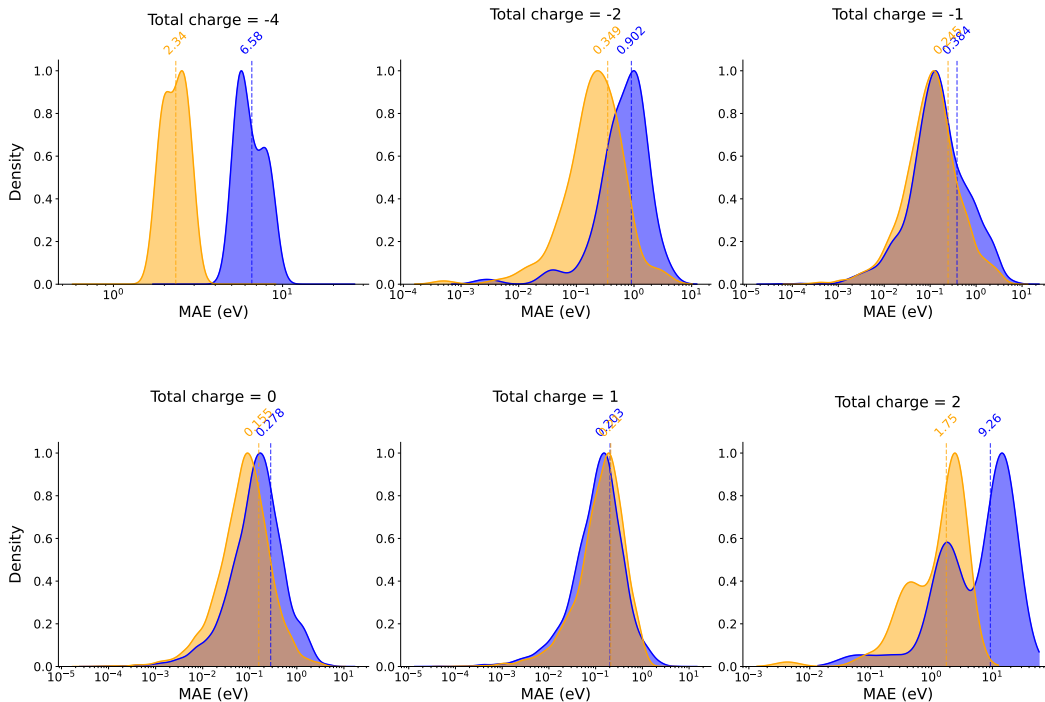


Figure 4: Evaluation of energy MAE distribution per global charge. A comparison of energy predictions of two equivalent ViSNet models, one trained with global charge embedding (yellow) and one without (blue), on the PmechDB dataset [72]. The distributions were obtained by evaluating the test split of the PmechDB dataset, which was used to train both models and contains around 10,000 structures with a similar charge distribution to the training split. Note that the total charge of -3 is absent from the evaluation data. The mean of each distribution is indicated by a colored vertical dashed line, and the value is displayed on top.

volume fluctuations and consequent sampling of an incorrect ensemble [62, 76]. The oxygen–oxygen radial distribution function $g_{OO}(r)$ is indistinguishable across all four NPT methods (5 panel c). Together, these results establish that both JAX-based NPT integrators included in this release sample equivalent NPT statistics to alternative commonly used algorithms. Finally, we note that our JAX-MD integrator is by far the fastest evaluated in this comparison, attaining speedups of 2.2x, 2.4x and 4.0x over our ASE integrator, *MelchionnaNPT* and *BerendsenNPT* respectively.

E Dataset and training details for pre-trained models

A curated version of the SPICE2 subset of OMOL25 [65] was created by removing chemically invalid structures (based on atomic valence heuristics) and entries where either the per-atom force norm or the total force exceeded a threshold of 0.1 eV/Å and 15 eV/Å, respectively. For model training, this dataset was split into training, validation and test sets using a 90:9:1 ratio. To prevent different conformers of the same molecule from being present in both sets, the split was performed on the SMILES strings.

The final training set contains 1,763,962 structures covering 17 chemical elements (B, Br, C, Ca, Cl, F, H, I, K, Li, Mg, N, Na, O, P, S, Si), the validation set 172,838 structures across 17 elements, while the test set contains 17,477 structures across 13 elements. Each pre-trained model was trained for 220 epochs using NVIDIA H100 GPUs and a mean-squared-error loss. The full details of the model architectures and training hyperparameters can be found in Appendix F.

Compared to the pre-trained models released with *mip v1*, we introduce several important modifications to both the training data and procedure. On the data side, training is now conducted on a

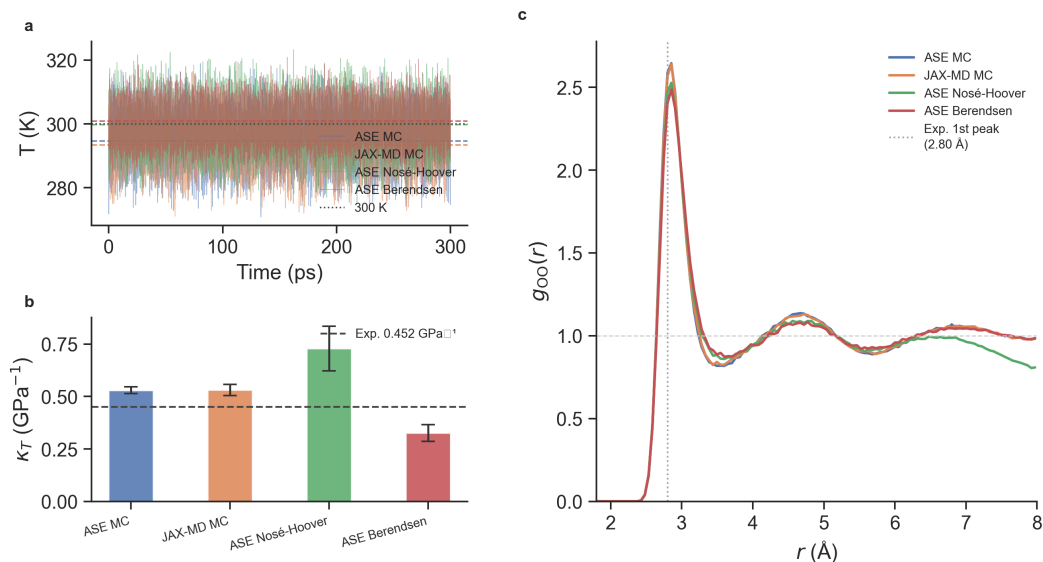


Figure 5: NPT molecular dynamics validation for VisNet-v2 water (501 molecules, 300 K, 1 atm). (a) Instantaneous temperature during the production run for each barostat; dashed lines show time averages, dotted line the target of 300 K. (b) Isothermal compressibility κ_T estimated from volume fluctuations; error bars are standard errors from 10-block averaging; the dashed line marks the experimental value of 0.452 GPa^{-1} [75]. (c) Oxygen-oxygen radial distribution function $g_{OO}(r)$; the dotted vertical line indicates the experimental first-peak position at 2.80 \AA [77].

curated version of the SPICE2 subset of OMOL25 [65], replacing the original SPICE dataset, and now explicitly includes charged systems. The chemical coverage is also expanded, increasing the number of supported elements from 15 to 17 through the addition of Ca and Mg. Furthermore, all models are extended to predict atomic partial charges alongside energies and forces.

F Model and training hyperparameters

The models were trained using very similar training strategies to v1, and to each other. Training was performed over 220 epochs with scheduled MSE loss weights: energy (40) and forces (1000), flipped at epoch 115. The charge weight (1) stayed constant throughout, and the partial charge weight flipped at epoch 115 from 4 to 0.2. An exponential moving average (EMA) with decay rate 0.99 was applied. The AMSGrad variant of Adam optimizer was used. The exponential moving average of the weights is taken at every training step. We use 4000 warmup steps followed by 360000 transition steps. Gradient clipping was performed with a norm of 500, and no gradient accumulation was applied. See Table 2 for the hyperparameters used for the NequIP model, Table 3 for ViSNet, Table 4 for MACE and Table 5 for eSEN. All training was done on NVIDIA H100 GPUs.

G MLIPAudit benchmark results

Table 6 reports per-benchmark scores for all four pre-trained models released with this library, following the MLIPAudit category structure: General, Small Molecules, Molecular Liquids, and Biomolecules. eSEN and ViSNet results are complete (14 scored benchmarks); MACE and NequIP results are partial at the time of writing, with sampling, stability, solvent and water radial distribution, and tautomers still in progress.

General. All models achieve strong stability scores (≈ 0.90), confirming well-behaved potential energy surfaces across the molecular systems tested.

Table 2: NequIP model hyperparameters.

Parameter	Value
num_layers	5
target_irreps	64x0e + 64x0o + 32x1o + 32x1e + 32x2e + 32x2o
l_max	2
num_rbf	8
radial_net_nonlinearity	swish
radial_net_n_hidden	64
radial_net_n_layers	2
radial_envelope	polynomial_envelope
mlp_variance_scale	4.0
embed_activation	silu
predict_partial_charges	True
use_total_charge_embedding	True
use_coulomb_term	False
graph_cutoff_angstrom	5.0
batch_size	128
learning_rate	2e-3

Table 3: ViSNet model hyperparameters.

Parameter	Value
num_layers	4
num_channels	128
l_max	2
num_heads	8
num_rbf	32
trainable_rbf	False
activation	silu
attn_activation	silu
embed_activation	silu
vecnorm_type	None
predict_partial_charges	True
use_total_charge_embedding	True
use_coulomb_term	False
graph_cutoff_angstrom	5.0
batch_size	128
learning_rate	1e-3

Small Molecules. This is the most densely evaluated category. All models score perfectly on bond length distributions and ring planarity, and achieve near-perfect scores on reference geometry stability (1.000 for eSEN, MACE, and NequIP; 0.995 for ViSNet). Conformer selection scores range from 0.875 to 0.946, and dihedral scan scores from 0.633 to 0.704. Non-covalent interactions are moderate (0.548–0.652), with eSEN leading. The most challenging benchmarks in this category are tautomers (0.07–0.10), nudged elastic band (0.16–0.24), and reactivity (0.21–0.28), all of which require accurate treatment of transition states and proton-transfer processes that are underrepresented in current training data.

Molecular Liquids. eSEN and ViSNet both reproduce water and solvent radial distribution functions with high fidelity (0.936–1.000), indicating well-calibrated short-range interactions in condensed-phase environments.

Biomolecules. Folding stability scores cluster around 0.53 across all models, suggesting systematic underestimation of long-range conformational preferences. Sampling scores of 0.744 (eSEN) and 0.781 (ViSNet) indicate physically meaningful free-energy landscapes for small peptides.

Table 4: MACE model hyperparameters.

Parameter	Value
num_layers	2
num_channels	128
l_max	3
node_symmetry	2
correlation	2
readout_irreps	["16x0e", "0e"]
num_readout_heads	1
num_rbf	16
activation	silu
embed_activation	silu
radial_envelope	polynomial_envelope
gate_nodes	True
include_pseudotensors	False
symmetric_contraction_backend	e3j
predict_partial_charges	True
use_total_charge_embedding	True
use_coulomb_term	False
graph_cutoff_angstrom	5.0
batch_size	128
learning_rate	2e-3

Table 5: eSEN model hyperparameters.

Parameter	Value
num_layers	2
sphere_channels	128
hidden_channels	128
edge_channels	128
l_max	2
m_max	2
num_rbf	32
rbf_type	gauss
basis_width_scalar	2.0
radial_envelope	polynomial_envelope
trainable_rbf	False
norm_type	rms_norm_sh
act_type	gate
embed_activation	silu
cosine_cutoff	False
predict_partial_charges	True
use_total_charge_embedding	True
use_coulomb_term	False
graph_cutoff_angstrom	5.0
batch_size	128
learning_rate	1.5e-3

† Partial results: overall scores averaged over completed benchmarks only.

H Additional validation and performance metrics for pre-trained models

In Figure 6, we present the corresponding RMSE error metrics for the MAE metrics presented in Figure 2 of the main text. Furthermore, Figure 7 shows the MAE and RMSE metrics for the partial charge predictions of the pre-trained models (MACE, NequIP, ViSNet, and eSEN).

Table 6: MLIPAudit benchmark scores (fast run mode), grouped by category. — denotes benchmarks not yet completed; n/s denotes benchmarks without a numeric score.

Benchmark	ESEN	ViSNet	MACE [†]	NequIP [†]
<i>General</i>				
Stability	0.900	0.900	—	—
Scaling	n/s	n/s	n/s	n/s
<i>Small Molecules</i>				
Bond length distribution	1.000	1.000	1.000	1.000
Ring planarity	1.000	1.000	1.000	1.000
Reference geometry stability	1.000	0.995	1.000	1.000
Conformer selection	0.946	0.913	0.898	0.875
Dihedral scan	0.704	0.687	0.640	0.633
Noncovalent interactions	0.652	0.566	0.561	0.548
Nudged elastic band	0.200	0.180	0.160	0.240
Reactivity	0.268	0.217	0.278	0.211
Tautomers	0.099	0.074	—	—
<i>Molecular Liquids</i>				
Water radial distribution	0.995	1.000	—	—
Solvent radial distribution	0.995	0.936	—	—
<i>Biomolecules</i>				
Folding stability	0.529	0.532	0.531	0.529
Sampling	0.744	0.781	—	—
Overall	0.716	0.699	0.674	0.671

Furthermore, we evaluate the runtime performance of the different pre-trained models on MD simulations using both the JAX-MD and ASE backends (Table 7). All benchmarks were conducted on a single NVIDIA H100 GPU, and the results span two representative systems: 1UAO, a small chignolin molecule comprising 138 atoms, and 1ABT with 1205 atoms. More details about these test systems, as well as their visualization can be found in the *mlip* v1 publication [1]. Across both backends and system sizes, all evaluated models maintain stable MD trajectories. We note that the reported runtimes are not directly comparable to their *mlip* v1 counterparts due to differences in hyperparameter settings.

Table 7: Speed performance on MD simulation of the different pre-trained models for the JAX-MD and ASE simulation backends. All tests were run on a single NVIDIA H100 GPU, and speed metrics are given in milliseconds per step, averaged over 1 ns of simulation. 1UAO is a chignolin molecule with 138 atoms, while 1ABT is a system with 1205 atoms. All models included in the table achieved stable simulations on these benchmarks. Note that the model runtimes cannot be compared directly to their *mlip* v1 counterparts due to different hyperparameters.

Models	Parameters	Systems	JAX-MD	ASE
MACE	3,274,016	1UAO	2.4 ms/step	7.3 ms/step
		1ABT	19.2 ms/step	43.8 ms/step
NequIP	1,921,280	1UAO	3.4 ms/step	8.9 ms/step
		1ABT	22.0 ms/step	44.6 ms/step
ViSNet	1,172,676	1UAO	1.9 ms/step	7.1 ms/step
		1ABT	13.7 ms/step	30.2 ms/step
eSEN	3,210,498	1UAO	3.0 ms/step	8.9 ms/step
		1ABT	22.8 ms/step	46.7 ms/step

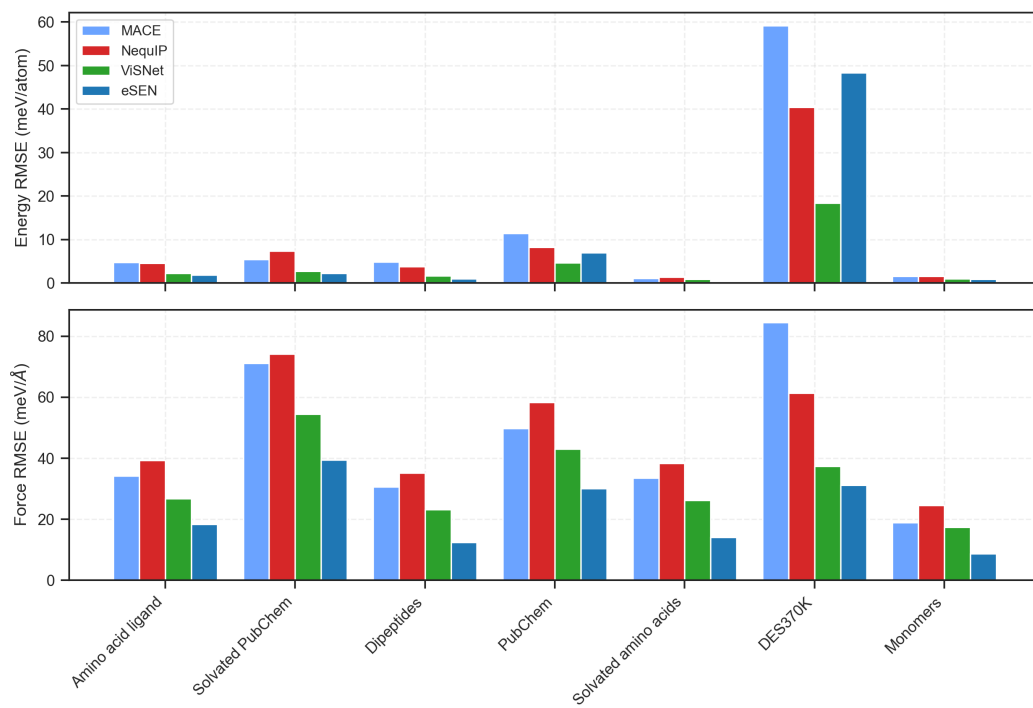


Figure 6: Validation set root-mean-squared errors (RMSE) for energy per atom (meV/atom) and atomic forces (meV/Å) across seven molecular subsets in the SPICE2 subset of the OMOL25 dataset. The four pre-trained models MACE, NequIP, ViSNet, and eSEN are evaluated. The subsets include: amino acid ligands, solvated PubChem, dipeptides, PubChem, solvated amino acids, DES370K and monomers. RMSE values reflect the deviation from DFT reference calculations.

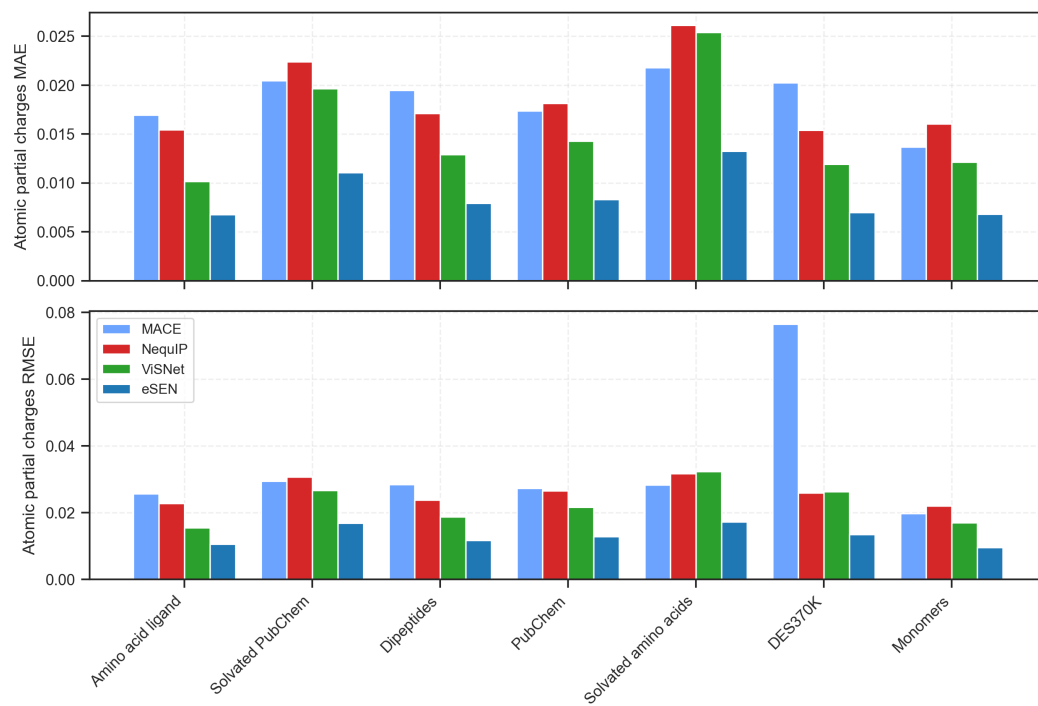


Figure 7: Validation set mean absolute errors (MAE) and root-mean-squared errors (RMSE) for atomic partial charge predictions across seven molecular subsets in the SPICE2 subset of the OMOL25 dataset. The four pre-trained models MACE, NequIP, ViSNet, and eSEN are evaluated. The subsets include: amino acid ligands, solvated PubChem, dipeptides, PubChem, solvated amino acids, DES370K and monomers. MAE and RMSE values reflect the deviation from DFT reference calculations.